

1 **Skeletal muscle dysfunction is associated with derangements in mitochondrial**
2 **bioenergetics (but not UCP3) in a rodent model of sepsis**

3

4 **Parjam Zolfaghari^{1,3}, Jane E Carré¹, Nadeene Parker³, Nancy A Curtin², Michael R Duchon³,**
5 **Mervyn Singer¹.**

6 1 Bloomsbury Institute for Intensive Care Medicine, University College London, Cruciform
7 Building, Gower Street, London WC1E 6BT, UK

8 2 National Heart and Lung Institute, Imperial College London, London, UK

9 3 Department of Cell and Developmental Biology, University College London, Gower
10 Street, London WC1E 6BT, UK

11

12 **Corresponding author:**

13 Parjam S Zolfaghari

14 Current address: Adult Critical Care Unit, 4th Floor, Royal London Hospital, Barts Health NHS
15 Trust, Whitechapel, London E1 1BB

16 Email: parjam.zolfaghari@bartshealth.nhs.uk

17 Tel. +44 (0) 7712673051

18

19

20 **Authors' details:**

21 **Parjam S Zolfaghari**

22 **Email:** parjam.zolfaghari@bartshealth.nhs.uk

23 **Contribution:** Conceived, designed and carried out experiments, analysed data and wrote
24 manuscript

25

26 **Jane E Carré**

27 **Email:** J.E.Carre@exeter.ac.uk

28 **Contribution:** Designed experiments, analysed data, wrote manuscript

29

30 **Nadeene Parker**

31 **Email:** nadeenestewart@gmail.com

32 **Contribution:** Designed experiments and analysed data

33

34 **Nancy Curtin**

35 **Email:** n.curtin@imperial.ac.uk

36 **Contribution:** Designed experiments, provided facilities and analysed data

37

38 **Michael R Duchon:**

39 **Email:** m.duchon@ucl.ac.uk

40 **Contribution:** Conceived and designed experiments, provided facilities and wrote manuscript

41

42 **Mervyn Singer**

43 **Email:** m.singer@ucl.ac.uk

44 **Contribution:** Conceived and designed experiments, provided facilities and wrote manuscript

45

46 All authors revised and approved final draft.

47

48 **Abstract:**

49 Muscle dysfunction is a common feature of severe sepsis and multi-organ failure. Recent
50 evidence implicates bioenergetic dysfunction and oxidative damage as important underlying
51 pathophysiological mechanisms. Increased abundance of uncoupling protein-3 (UCP-3) in
52 sepsis suggests increased mitochondrial proton leak, which may reduce mitochondrial
53 coupling efficiency but limit ROS production. Using a murine model, we examined metabolic,
54 cardiovascular and skeletal muscle contractile changes following induction of peritoneal
55 sepsis in *wild-type* and *Ucp3^(-/-)* mice. Mitochondrial membrane potential ($\Delta\psi_m$) was
56 measured using two-photon microscopy in living diaphragm, and contractile function was
57 measured in diaphragm muscle strips. The kinetic relationship between membrane potential
58 and oxygen consumption was determined using a modular kinetic approach in isolated
59 mitochondria. Sepsis was associated with significant whole body metabolic suppression,
60 hypothermia and cardiovascular dysfunction. Maximal force generation was reduced and
61 fatigue accelerated in *ex vivo* diaphragm muscle strips from septic mice. Mitochondrial
62 membrane potential was lower in the isolated diaphragm from septic mice despite normal
63 substrate oxidation kinetics and proton leak in skeletal muscle mitochondria. Even though
64 wild-type mice exhibited an absolute $26 \pm 6\%$ higher UCP-3 protein abundance at 24 hours,
65 no differences were seen in whole animal or diaphragm physiology, nor in survival rates,
66 between wild-type and *Ucp3^(-/-)* mice. In conclusion, this murine sepsis model shows a
67 hypometabolic phenotype with evidence of significant cardiovascular and muscle
68 dysfunction. This was associated with lower $\Delta\psi_m$ and alterations in mitochondrial ATP
69 turnover and phosphorylation pathway. However, UCP-3 does not play an important
70 functional role, despite its upregulation. (246 words)

71 **Keywords:** Sepsis, Mitochondria, Metabolism, Uncoupling protein 3, Skeletal
72 muscle

73

74 **Glossary**

- 75 **i/p** Intraperitoneal
- 76 **$\Delta\Psi_m$** Mitochondrial membrane potential
- 77 **RER** Respiratory exchange ratio
- 78 **s/c** Subcutaneous
- 79 **SDS** Sodium dodecyl sulfate
- 80 **TMRM** Tetramethylrhodamine methyl ester
- 81 **TPMP** Methyltriphenylphosphonium
- 82 **UCP** Uncoupling protein
- 83 **VO₂** Whole body oxygen consumption
- 84 **VCO₂** Whole body carbon dioxide production
- 85 **WT** Wild-type
- 86
- 87

88 Introduction

89 Muscle dysfunction is a common feature of severe sepsis and other critical illnesses,
90 and a major cause of both prolonged intensive care stay (21) and long-term disability (7, 34).
91 Neuropathic and myopathic features are well recognized (7, 38, 40, 50), yet the underlying
92 pathophysiology remains incompletely understood. A net catabolic state, impaired cellular
93 and calcium signalling, bioenergetic dysfunction and oxidative damage are all implicated (30,
94 33, 50). In both patients and animal models, sepsis is associated with decreased skeletal
95 muscle mitochondrial respiratory capacity, reduced mitochondrial protein levels and
96 increased rates of generation of reactive oxygen and nitrogen species (ROS and RNS) (12, 13,
97 16, 18, 20, 26), all of which may impair muscle function.

98 The proton electrochemical gradient created by activity of the mitochondrial
99 respiratory chain generates a transmembrane potential ($\Delta\psi_m$) that is used by the F_0F_1 ATP
100 synthase to phosphorylate ADP to ATP (coupled respiration). However, a variable proportion
101 of protons are uncoupled from ATP synthesis by leaking back into the mitochondrial matrix,
102 the rate of proton flux being dependent upon the magnitude of $\Delta\psi_m$. Proton leak rate is
103 variable and considered to constitute ~20% of the basal metabolic rate of hepatocytes, and
104 up to 50% in rat skeletal muscle (53). Uncoupled respiration has basal and inducible
105 components (35), with the inducible part forming the mechanism of heat generation in
106 brown adipose tissue through uncoupling protein (UCP)-1 (44). Other uncoupling proteins –
107 UCP-2-5 – have been identified but their physiologic role and biochemical mechanisms
108 remain controversial. One suggestion is that following activation by ROS and by-products of
109 ROS damage, these UCPs may induce a mitochondrial proton leak (11, 25) that, in turn, may
110 down-regulate ROS production, forming a negative feedback loop (42).

111 Processes interfering with maintenance of $\Delta\psi_m$ may impact on cellular energy supply
112 and mitochondrial ROS production (23, 45). Sepsis is associated with high levels of nitric
113 oxide production which impairs respiratory enzyme function (12, 27). Increased expression

114 of UCP-2 and UCP-3, reported in septic mouse models (60, 66), suggests a possible increase
115 in proton leak with a reduction in mitochondrial coupling efficiency (the proportion of
116 mitochondrial oxygen consumption used to drive ATP synthesis). A consequential decrease in
117 mitochondrial ATP production could have significant impact on muscle contractile function.

118 The traditional approach of measuring whole body oxygen consumption as a marker
119 of metabolic rate in sepsis does not take into account the proportion of oxygen use that is
120 uncoupled from oxidative phosphorylation. This proportion may fluctuate considerably over
121 time, particularly in view of the significant thermoregulatory and inflammatory disturbances
122 that occur in this condition.

123 The aim of our study was to determine changes in metabolism, muscle function and
124 the influence of UCP3 in an established rodent model of sepsis. We hypothesised that sepsis
125 leads to metabolic suppression and muscle dysfunction as a result of decreased capacity of
126 mitochondrial ATP synthesis, and that UCP3, an uncoupling protein restricted to muscle and
127 adipose tissue, offers protection to ROS-induced muscle contractile dysfunction at the
128 expense of mitochondrial efficiency.

129

130

131 **Methods**

132 **Mouse septic model.** All experiments were performed under the UK Animals (Scientific
133 Procedures) Act 1986 with approval from the University College London Ethics Committee.
134 Ten-week old male C57 black mice were purchased from Charles River (Margate, UK) and
135 maintained in the university animal facility until they reached 25-35 weeks of age. They were
136 housed in cages (maximum 6 per cage) with standard bedding, environment-enhancing
137 objects and free access to water and chow diet. Cages were maintained at room
138 temperature with 12-hour light and dark cycles. Comparison was made against age-matched
139 litter mice from three *Ucp3*^(-/-) homozygote breeding pairs (originally produced by Gong *et al*
140 (29) and back-crossed ten generations with wild-type C57 mice). Confirmatory genotyping
141 was carried out using tail snips. All *Ucp3*^(-/-) mice were kept in individually ventilated cages
142 with litter-mates of the same sex kept in the same cage after weaning. Mice were allowed to
143 acclimatize to the laboratory for one week prior to the start of experiments.

144 The model of sepsis has been described in detail elsewhere (67). In summary, sepsis
145 was induced by intraperitoneal injection of diluted cecal slurry (20 ml/kg) under a brief
146 period of isoflurane anesthesia. Sham mice received 20 ml/kg of 0.9% saline i/p. As septic
147 mice stop eating, a further sham starved group was added to account for this potential
148 confounding factor. Starvation commenced after i/p injection of saline. Mice were block-
149 randomized to each treatment group for each set of experiments.

150 All mice received 0.9% saline 10ml/kg s/c at time 0 h, and 50 ml/kg of 5%
151 dextrose/0.81% saline solution at 6, 18, 30 and 42 h. Initial experiments observed 72-hour
152 survival, serum biochemical markers of organ failure, blood gases and echocardiography
153 (Vivid 7, GE Healthcare, Chalfont St. Giles, Bucks, UK) at 24 hours. Clinical variables
154 comprising behaviour, appearance temperature and acidemia were used to score sepsis
155 severity (67). Severity scoring was carried out by two observers, one of whom was blinded to

156 the randomization process. The scores given by the two observers were consistently equal.

157 Subsequent studies are outlined below.

158 **Whole animal metabolism.** Whole body metabolic rate of sham and septic mice were
159 measured for 24h in individual metabolic chambers (Oxymax, Columbus Instruments,
160 Columbus, OH). Gas samples from each box were sampled for 90 seconds at 8-minute
161 intervals. Oxygen consumption (VO_2) and CO_2 production (VCO_2) were calculated using
162 standard formulae. The respiratory exchange ratio (RER) was calculated as the ratio of VCO_2
163 to VO_2 . Values near 1 indicate a predominance of carbohydrate metabolism while values
164 approaching 0.7 indicate fatty acid oxidation (36). Rectal temperature was measured at 0, 6,
165 18 and 24h, and animals were weighed at 0 and 24h time-points.

166 **Assessment of cardiac function:** Echocardiography was performed at 0, 6 and 24h in sham
167 and septic *wild-type* and *Ucp3^(-/)* mice using a 14 MHz probe connected to a Vivid 7
168 Dimension device as previously described (67). Aortic blood flow velocity was measured in
169 the proximal ascending aorta immediately before the bifurcation of the right carotid artery
170 using pulse-wave Doppler. Stroke volume was calculated by multiplying the velocity time
171 integral (VTI) from six consecutive cycles (equivalent to one respiratory cycle) by aortic cross-
172 sectional area (using an aortic diameter of 0.26 cm). Average peak-to-peak distance and
173 maximum velocity over six consecutive systolic cycles were used to measure heart rate and
174 peak velocity, the latter being a marker of left ventricular contractility (12). Cardiac output
175 was calculated as the product of stroke volume and heart rate.

176 **Western blotting for UCP3 protein.** UCP-3 protein abundance was measured in snap-frozen
177 heart and skeletal muscle tissue at 10 and 24h following induction of sepsis in the *wild-type*
178 mice. After SDS protein precipitation, 10 μ g protein was separated on a 12% SDS
179 polyacrylamide gel and transferred to nitrocellulose. Membranes were probed overnight at
180 4°C with the primary antibody (Rabbit anti-UCP3: PA1-055 Pierce antibodies, ThermoFisher

181 Scientific, Loughborough, Leics, UK) at 1:1000 dilutions in blocking buffer. Each sample was
182 loaded twice in the same gel, and each gel repeated once. Following incubation with
183 secondary antibody (goat-anti-rabbit antibody: DAKO, Ely, Cambs, UK), cross-reacted
184 proteins were visualised by enhanced chemiluminescence (Amersham Biosciences, Little
185 Chalfont, Bucks, UK). Densitometry measurements were made using Image J image
186 processing and National Institute of Health analysis software. A single control sample was
187 used in each gel and all results normalized to this control allowing comparison between
188 samples in different gels. Alpha-tubulin (1:5000 dilution, Abcam 7291, Cambridge, Cambs,
189 UK) was used to ensure equal loading of gels and transfer of proteins from gel to membrane.
190 Each membrane was also Coomassie stained to ensure equal loading and transfer.

191 **Diaphragm preparation.** At 24h, under terminal isoflurane anesthesia, a midline laparotomy
192 was performed and the diaphragm excised *en-bloc* (still attached to ribs laterally) and pinned
193 (taut without excess stretch) at its edges in a petri dish filled with physiological saline
194 (containing of mmol/L: Na^+ 145, K^+ 5, Ca^{2+} 5, Mg^{2+} 1, HCO_3^- 25, Cl^- 118, SO_4^{2-} 1, PO_4^{3-} 1,
195 glucose 10, pyruvate 10, and equilibrated with 95% O_2 and 5% CO_2 (pH 7.4). Tubocurarine
196 (2.5 μm) was added to stop spontaneous neuromuscular junction activity. Diaphragm strips
197 (~1 mm wide) were dissected using stereomicroscopy; a strip consisted of muscle fibers with
198 the ribs at one end and central tendon at the other. Strips were allowed to rest in
199 physiological saline for at least 30 minutes prior to experimentation. All experiments were
200 performed within 5h of tissue harvest.

201 **Force and power measurements.** Aluminium foil T-clips were attached to the rib and central
202 tendon at the ends of the diaphragm strips using cyanoacrylate gel glue. The muscle strips
203 were transferred to a temperature-controlled (23°C) Perspex bath through which
204 physiological saline was continuously circulated. At one end the strip was attached to a
205 combined motor and force transducer (Model 300B, Cambridge Technology, Inc.,
206 Watertown, MA, USA) and the other end to a hook mounted onto a micrometer allowing

207 alteration of resting muscle length. Electrical stimulation (MultiStim System-D330, Digitimer,
208 Welwyn Garden City, Herts, UK) was delivered by two platinum electrodes placed in the bath
209 just above and below the belly of the muscle fibres. A program written in TestPoint (Keithley
210 Instruments, Bracknell, Berks, UK) controlled stimulation and motor arm position and
211 recorded force, length and stimulation. A DAS-1800AO Series A/D board (Keithley
212 Instruments) was used. The computer program could be altered to achieve complex
213 protocols such as force recording during repeated phased cyclical tetanic stimulations while
214 making controlled changes to muscle length.

215 Following system calibration and zeroing, optimal stimulation voltage (at 96Hz) was
216 found for the muscle strip; these stimulus parameters were used throughout the
217 experiment. The length/tension relationship was explored by increasing the muscle length in
218 0.2-0.4 mm increments to identify L_0 , the muscle length at which filament overlap was
219 optimal for isometric tetanic force development. A single 350 ms tetanic stimulation was
220 used to measure the maximal achievable tetanic isometric force. The maximum force
221 generated was expressed relative to muscle cross-sectional area (CSA) to take account
222 muscle size.

$$223 \quad \text{CSA} = 4.9 \times d \times M / L_0$$

224 where 4.9 is the wet-to-dry ratio (65), d is density (assumed to be 1 mg/mm^3), M is dry mass
225 of the muscle and L_0 is muscle length as defined above. M and L_0 were measured at the end
226 of the experiment.

227 The ability of the muscle to produce work and power was measured using a pattern
228 of sinusoidal movement and stimulation that mimics diaphragm muscle action *in vivo*. This
229 pattern was described and optimized by Stevens and Faulkner for diaphragm muscle strips
230 from C57 black mice (59). The amplitude of the length change was $\pm 0.4 \text{ mm}$. Stimulation was
231 applied for $\sim 30\%$ of each movement cycle and was approximately centered on the time at

232 which the muscle length was longest. The maximum power was measured in one cycle of
233 movement at frequency 4Hz. The initial muscle strip length was incrementally increased to
234 find optimal range. To measure the effects of fatigue on power, cycles of length change with
235 stimulation were repeated over a one-minute period. The frequency of movement was 2 Hz,
236 which is equivalent to 120 breaths/min, close to the average respiratory rate measured in
237 septic mice.

238 The net work performed by the muscle strip is the 'positive work' performed during
239 muscle shortening and contraction, minus the 'negative work' to bring the muscle back to its
240 original length (59). We evaluated net work as follows: Passive force was recorded during
241 movement without electrical stimulation, and then during the same movement with
242 electrical stimulation. The unstimulated record was subtracted from the stimulated record to
243 give the active force value. Net work performed during the movement cycle was evaluated
244 as the area circumscribed by the active force vs. length change graph, referred to as work
245 loop (Fig. 5C). The average power output during the movement cycle was calculated by
246 dividing net work by cycle duration, and is expressed relative to the muscle strip wet weight
247 to take account of size.

248 ***Diaphragm muscle mitochondrial membrane potential ($\Delta\psi_m$)***. Diaphragm muscle strips (3-4
249 mm wide) taken at 24h from paired fed sham and septic wild-type mice were pinned onto a
250 Sylgard™ imaging chamber and continuously superfused with oxygenated saline solution at
251 23°C on the stage of an upright epifluorescent microscope (Zeiss Axioskop, Carl Zeiss,
252 Cambridge, Cambs, UK) with a x63 Achroplan water dipping objective and 0.9 numerical
253 aperture. The strips were incubated for 45 min with the lipophilic cationic dye,
254 tetramethylrhodamine methyl ester (TMRM) (Invitrogen, Paisley, Renfrewshire, UK) added to
255 the circulating saline solution at low concentration (100 nM). Fluorophore excitation was
256 achieved using a femtosecond pulsed Ti:sapphire tunable multiphoton laser (Coherent
257 Chameleon, Santa Clara, CA) set at wavelength 720nm. A photomultiplier tube detected the

258 emitted light, which was first split by a long pass 510nm dichroic mirror before passing
259 through a band pass filter 560-615nm.

260 Accumulation of TMRM in cells and mitochondria depends on both plasma
261 membrane potential and $\Delta\psi_m$. At low loading concentrations, TMRM fluorescence intensity
262 is linear to its concentration (24). The baseline fluorescence intensity of TMRM in muscle
263 strips isolated from sham and septic mice was measured and directly compared.
264 Fluorescence intensity was also determined in the presence of the ATP synthase inhibitor,
265 oligomycin (10 $\mu\text{g/ml}$, Sigma-Aldrich, Gillingham, Dorset, UK) and the protonophore,
266 carbonyl cyanide 4-(trifluoromethoxy) phenylhydrazone (FCCP) (1 μM , Sigma-Aldrich). The
267 addition of oligomycin can differentiate states where mitochondria are depolarized as a
268 result of high ATP production and flux through the respiratory chain, from other states
269 where a pathological process has resulted in ATP synthase to switch back to its native ATPase
270 activity (17, 28). The addition of FCCP results in dissipation of $\Delta\psi_m$, confirming that the
271 TMRM signal is truly mitochondrial and unquenched.

272 Stepped z-stacked images (10 at 4 μm apart) were taken in all three states (baseline,
273 after oligomycin, after FCCP) and assimilated to form a single projection for measurement of
274 TMRM fluorescence intensity. Three different fields of muscle cells corresponding to the
275 brightest regions of the muscle strip with at least 5 cells per field were analyzed using Zeiss
276 LSM software, and values from the three fields averaged to give a single result per specimen.
277 As it was unclear how $\Delta\psi_m$ would vary between subjects and in sepsis, eight subjects per
278 group were arbitrarily chosen. Statistical comparison was made within the group (i.e. sham
279 or septic) using ANOVA with repeated measures, and between groups using Student's t-test
280 for each state (baseline, +oligomycin, +FCCP).

281

282 **Isolation of mitochondria from total skeletal muscle.** At the 24h time-point, lower limb,
283 back and respiratory skeletal muscle were taken from *wild-type* fed sham, starved sham and
284 septic mice, with clinical severity scoring performed beforehand. Mitochondria were then
285 isolated as described by Bhattacharya *et al* (8) at 4°C. In brief, muscles were rapidly removed,
286 weighed and placed in ice-cold isolation solution (KCl 100mM, Tris/HCl 50mM, EGTA 2mM,
287 pH 7.4 at 4°C). The muscle was minced and the muscle slurry washed and protease-digested
288 in digestion buffer (KCl 100mM, Tris/HCl 50mM, EGTA 2mM, ATP 1mM, MgCl₂.6H₂O 5mM,
289 Defatted Bovine Serum Albumin 0.5%, Protease Type VIII [(245.7units/100ml, Sigma P
290 5380)], pH 7.4). The mixture was Dounce homogenized and spun for 10 min at 490g.
291 Supernatant was filtered and spun in 2-3 stages for 10 min each at 10,400g. The final pellet
292 (mitochondria) was resuspended in a small volume of isolation medium (0.6-0.8 ml) and
293 protein concentration measured using a BCA protein assay kit (ThermoFisher Scientific).

294 To determine percentage recovery of mitochondria from skeletal muscle homogenate from
295 all three groups of mice, citrate synthase activity was assayed at each step of the isolation
296 process by spectrophotometric determination of oxaloacetate-dependent coenzyme A-
297 coupled reduction of DTNB at 412nm (57), in an assay adapted for 96-well plates.

298 **Respiratory activity of isolated mitochondria and modular kinetic analysis.** Respiratory
299 activity of isolated mitochondria was determined using a Clark electrode chamber (Rank
300 Brothers, Bottisham, Cambs, UK) surrounded by a thermostatically-controlled water jacket at
301 30°C and calibrated with air-saturated assay medium. Mitochondria (0.35mg/ml) were
302 incubated in assay medium (KCl 120mM, KH₂PO₄ 5mM, HEPES 3mM, EGTA 1mM, 0.3% (w/v)
303 de-fatted BSA, pH 7.4).

304 Respiratory control ratios were calculated as state 3 respiratory rate after addition of
305 ADP (200µM) divided by the state 4 rate after ADP phosphorylation with pyruvate 5mM and
306 malate 2.5mM as substrates. Ratios of 3-10 have been quoted as acceptable RCR ratios (51,

307 58). FCCP (1-3 μ M) was added at end-study to measure maximal oxygen consumption rate; a
308 three-fold rise in respiratory rate has been used to indicate good mitochondrial quality (58).

309 **Modular kinetic analysis.** This technique allows interrogation of mitochondrial pathways
310 that generate $\Delta\psi_m$ (substrate oxidation), and pathways that utilize/dissipate it (proton leak
311 and ATP turnover) (10, 15, 47, 48). The conceptual division of mitochondrial respiration into
312 these three kinetic modules is further detailed in Figure 1. The modules are divided into a
313 substrate oxidation module ($\Delta\psi_m$ producing); an ATP turnover module, comprising
314 phosphorylation and associated transport activity ($\Delta\psi_m$ dissipating); and a proton leak
315 module ($\Delta\psi_m$ dissipating). Substrate oxidation and proton leak kinetics are determined
316 directly, while ATP turnover is derived by subtracting proton leak from total $\Delta\psi_m$ -dissipating
317 pathway activity. Studies were performed in a specially adapted 7 ml Clark electrode
318 chamber that simultaneously measures oxygen consumption and $\Delta\psi_m$ using a
319 methyltriphenylphosphonium (TPMP⁺) electrode in the presence of nigericin (0.1 μ M) to
320 abolish the pH gradient. Following addition of mitochondria (0.35 mg/ml) to the assay
321 medium (KCl 120mM, KH₂PO₄ 5mM, HEPES 3mM, EGTA 1mM, 0.3% (w/v) de-fatted BSA,
322 Nigericin 0.1 μ M; pH 7.4), the TPMP⁺ electrode was calibrated with five sequential 0.5 μ M
323 additions of TPMP. Mitochondria were energized with succinate 8mM (plus rotenone 5 μ M).
324 The starting oxygen level and the zero point were used for two-point calibration of the Clark
325 electrode (100% and 0% points). FCCP was added at the end of all experimental runs to
326 correct for any drift of the TPMP⁺ electrode. Due to the large number of mitochondria
327 needed for each of the protocols, mitochondria isolated from two mice in the same group
328 were pooled. Each protocol was run twice and the results averaged.

329 Since the kinetic response of each module to an effector reflects a change in the
330 common intermediate, $\Delta\psi_m$, the kinetic curves of modules that consume protonmotive force
331 are independent of the respiratory substrate used to generate that $\Delta\psi_m$ (2). Succinate (8

332 mM) was used as a substrate in all experiments, since mitochondrial energization is more
333 readily achieved than with NADH-linked substrates (41). The kinetic dependency of oxygen
334 consumption towards $\Delta\psi_m$ was described for each kinetic pathway module by modulating
335 $\Delta\psi_m$ using effectors targeted towards another module within the system. Substrate
336 oxidation kinetics were measured in the presence of oligomycin (1.3 μ M) by sequential
337 depolarization with FCCP (0.2-1 μ M). Proton leak kinetics were determined in the presence
338 of oligomycin 1.3 μ M by sequential additions of malonate (0.1–2.3 mM). The kinetics of total
339 $\Delta\psi_m$ -dissipating activity (proton leak + ATP turnover reactions) were measured under state 3
340 conditions (ADP 2 mM) by sequential additions of malonate (0.1–2.3 mM). ATP turnover
341 kinetics (phosphorylation and transport reactions) were subsequently calculated by
342 subtraction of proton leak rate from the state 3 respiratory rate at the corresponding value
343 of $\Delta\psi_m$. FCCP (1 μ M) was added at the end of all experimental runs to correct for drift of the
344 TPMP⁺ electrode.

345 To test for statistical significance, respiration rates between flanking values of $\Delta\psi_m$
346 were interpolated so that for each curve, oxygen consumption at $\Delta\psi_m$ of -170mV was
347 calculated. This value was the highest $\Delta\psi_m$ common to all conditions. The higher the value of
348 $\Delta\psi_m$, the higher the flux of protons through the various $\Delta\psi_m$ -consuming modules, and
349 therefore the more likely to see a result emerging through the inherent noise of the
350 experimental setup. Additionally, uncoupling proteins (UCP3 in particular) may require a high
351 $\Delta\psi_m$ to become active (48). One-way ANOVA was used to test for difference in VO_2 between
352 the groups at $\Delta\psi_m$ of -170mV.

353 ***Statistical analysis***

354 Statistical analysis was performed using SPSS 18.0 (IBM) software. Data were normally
355 distributed, unless stated. Student's t-test, Mann-Whitney U tests, and analysis of variance
356 (ANOVA) (with and without repeated measures calculations) were used to test for statistical

357 significance with the alpha error set to <5% ($p < 0.05$). Tukey and Dunnett *post hoc* tests were
358 used to define significance.

359

360 **Results**

361 **Whole body physiology and skeletal muscle function**

362 **Mortality and whole-animal metabolism.** Mortality rates of the septic wild-type (n=11) and
363 *Ucp3*^(-/-) mice (n=12) at 24h, 48h and 72h time-points were similar, at approximately 20%,
364 70% and 73%, respectively (Figure 2). No deaths occurred in either WT (n=10) or *Ucp3*^(-/-)
365 (n=9) sham groups. Septic mice developed a mixed respiratory and metabolic acidosis with
366 biochemical evidence of acute kidney and liver injury (Table 1). The degree of organ
367 dysfunction and acidosis correlated with severity of illness and mortality.

368 Sepsis produced a large and rapid drop in core temperature and metabolic rate with
369 good correlation between temperature and VO_2 ($R^2=0.95$) [Fig. 3A-C]. Responses were similar
370 in both wild-type and *Ucp3*^(-/-) groups. In both genotypes, the sham fed mice lost a small
371 amount of weight over the first 24 hours ($-2 \pm 1\%$ SEM body weight change; $p=0.08$). This was
372 more pronounced in the starved sham mice ($-8 \pm 1\%$ SEM body weight change; $p < 0.0001$).
373 However, the septic mice gained weight ($5 \pm 1\%$ SEM body weight; $p < 0.001$), due to a
374 combination of renal dysfunction and fluid sequestration in body cavities (pleural effusions
375 and ascites) and subcutaneous tissues evident at postmortem examination (Fig 3D).

376 **Cardiac function.** Echocardiography was performed in 16 sham and 13 severe septic *wild-*
377 *type* mice, and nine sham and seven severe septic *Ucp3*^(-/-) mice (Figure 4). Compared to
378 baseline values, there was a marked reduction in cardiac output at 6 and 24 h in the severe
379 septic mice in both genotypes ($p < 0.02$ within group ANOVA, but no statistical significance
380 between the two genotypes). Decreases were noted in left ventricular contractility

381 (measured as peak flow velocity), stroke volume and heart rate. No difference was seen
382 between wild-type and *Ucp3*^(-/-) groups.

383 **Diaphragm muscle force and power.** Measurements were made on diaphragm strips from
384 both wild-type (9 fed sham, 8 starved sham, 9 septic wild-type) and *Ucp3*^(-/-) (6 fed sham, 8
385 starved sham, 7 septic) mice. The average ages (\pm SEM) were 35 \pm 2 weeks for *wild-type* mice
386 and 35 \pm 3.5 weeks for *Ucp3*^(-/-) mice ($p=0.92$), with average weights of 32 \pm 4 and 34 \pm 3 g,
387 respectively ($p=0.048$). At 24h, maximal tetanic isometric force generated by diaphragm
388 strips from septic wild-type mice was 28% lower than that produced by either fed or starved
389 sham mice ($p<0.05$) (Fig. 5A). Similarly, maximal power generated during a single length cycle
390 at 4 Hz (mimicking 240 breaths/min, typical for normal mice) was 36% and 28% lower in
391 muscle strips from septic mice than from fed and starved sham mice, respectively ($p<0.05$
392 one-way ANOVA) (Fig. 5B). Similar results were seen in the muscle strips from *Ucp3*^(-/-)
393 animals (Figure 5A and B). The work loop profiles generated by all sets of muscle strips
394 showed a similar contraction-relaxation profile (Fig. 5C).

395 The effect of fatigue on power output was assessed during cycles of movement and
396 stimulation repeated for one minute. A movement frequency of 2 Hz was used to mimic the
397 respiratory rate of 120 breaths/min in a septic mouse. A characteristic pattern of power
398 fatigue was seen: an initial rapid decline was followed by a plateau phase, and then a second
399 rapid decline to a lower plateau (Fig. 5D). The initial power in the fatigue test (Fig. 5D) was
400 about half of the maximum power (shown in Fig. 5B) due to the difference in movement
401 frequency, 2 and 4 Hz respectively. For both genotypes, the power output throughout the
402 fatigue test was lower in the septic group than in either of the sham groups. For both
403 genotypes, the duration of the first plateau ended sooner in the septic group (35 \pm 3 cycles)
404 compared to both fed sham (41 \pm 6 cycles) and starved sham (41 \pm 4 cycles) strips ($p= 0.02$).

405 In summary, sepsis resulted in severe hypothermia and metabolic suppression
406 associated with cardiovascular dysfunction, lower muscle force and power generation, and
407 earlier fatigue. As no differences were seen between wild-type and *Ucp3*^(-/-) mice, this implies
408 that UCP3 does not affect the response to sepsis neither at the level of the whole animal nor
409 at the level of muscle (dys)function. Further experiments were thus performed using only
410 wild-type animals.

411 **Mitochondrial physiology**

412 A detailed analysis of mitochondrial function was performed to determine whether
413 mitochondrial dysfunction, potentially including increased proton leak, could underlie the
414 muscle dysfunction described above. Studies were performed using wild-type mice only.

415 **UCP protein abundance.** UCP3 protein expression in diaphragms taken from wild-type sham
416 (n=6) and severe septic mice (n=9) at 24h was assessed by Western blot. UCP3 protein
417 abundance increased by 26±6% (SEM) compared to sham (p<0.05). The α -tubulin
418 densitometry signal decreased in septic wild-type mouse diaphragms by 22±7% at 10h
419 [p=0.016], and by 12 ± 6% at 24h [NS]. The ratio of UCP3 to α -tubulin change was 47 ± 13%
420 (p<0.05; Figure 6). Coomassie staining confirmed equal protein loading and transfer. UCP2
421 was not detectable in these samples using 3 different commercially available antibodies.

422 **Mitochondrial membrane potential in diaphragm muscle strips.** Muscle strips from nine fed
423 sham and nine septic wild-type mice were compared simultaneously. TMRM loading took 45
424 minutes to reach steady state prior to imaging. A typical double row and subsarcolemmal
425 high intensity fluorescence pattern was observed in all muscle cells, representing
426 interfibrillar and subsarcolemmal groups of mitochondria (Figures 7A-C). Baseline TMRM
427 fluorescence in diaphragms from *wild-type* septic mice was significantly lower than
428 diaphragms from sham mice, suggesting a decrease in mitochondrial membrane potential
429 ($\Delta\Psi_m$) (Figure 7D). The ATP synthase inhibitor, oligomycin was then added to observe

430 changes in $\Delta\psi_m$ following inhibition of mitochondrial ATP production. This differentiates
431 between states where mitochondria are depolarized as a result of high ATP production and
432 flux through the respiratory chain, from other states where the ATP synthase switches into
433 its native ATPase activity (17, 28). In the diaphragm strips, oligomycin increased TMRM
434 fluorescence, with a greater relative increase above baseline in the septic group (increase of
435 $30 \pm 5\%$ in septic diaphragm vs $16 \pm 8\%$ in sham; $p < 0.001$). Absolute values of fluorescence
436 post-oligomycin were not statistically different between the two groups ($p = 0.1$), suggesting
437 the differences are attributable to a difference in proton flux through the F_0F_1 -ATP synthase.
438 The addition of FCCP resulted in complete dissipation of $\Delta\psi_m$ in all specimens examined,
439 confirming unquenched mitochondrial TMRM signal (24).

440 ***Citrate synthase activity and respiratory control of isolated mitochondria from skeletal***
441 ***muscle.*** Mitochondria were isolated from muscles of 8 fed sham, 8 starved sham and 13
442 severe septic wild-type mice (clinical severity 5-6). Fractional recovery (mean \pm SD) of citrate
443 synthase activity at each step of the mitochondrial preparation process compared to the
444 initial muscle homogenate was similar in all three groups, with a final recovery in the
445 mitochondrial pellet of $43 \pm 11\%$ (fed sham), $38 \pm 23\%$ (starved sham) and $41 \pm 9\%$ (septic)
446 ($p = 0.48$). The respiratory control of the final mitochondrial pellet measured using the NADH-
447 linked substrates pyruvate and malate was also similar (3.0 ± 0.6 fed sham, 3.5 ± 0.9 starved
448 sham, 2.9 ± 0.5 septic; $p = 0.47$).

449 ***Modular kinetic analysis of isolated skeletal muscle mitochondria.*** The effect of sepsis on
450 the kinetic behavior of processes that govern $\Delta\psi_m$ were examined using modular kinetic
451 analysis in 8 fed sham, 8 starved sham and 13 severe septic mice. Substrate oxidation ($\Delta\psi_m$
452 producing) and proton leak kinetics ($\Delta\psi_m$ consuming) were determined directly, while ATP
453 turnover ($\Delta\psi_m$ consuming) was derived by subtracting proton leak from total $\Delta\psi_m$ -
454 dissipating pathway activity. Proton leak kinetics were similar in all three groups (Figs 8 A,B).

455 However, the kinetic behavior of total $\Delta\Psi_m$ -dissipating processes (Figs 8 C,D) and ATP
456 turnover processes (Figs 8 E,F) were significantly affected in the septic mice: for a given
457 membrane potential (-170 mV), the oxygen consumption rate was significantly lower in
458 mitochondria from septic animals (207 ± 26 fed sham, 157 ± 53 starved sham, 120 ± 30 septic
459 nmol oxygen/min/mg; $p < 0.05$). While the substrate oxidation kinetic curves of the septic and
460 fed sham mice were similar (Figs 8 G,H), the curve for the starved sham group (316 ± 19 nmol
461 oxygen/min/mg) was significantly different compared to both fed sham (230 ± 17) and septic
462 (312 ± 22) groups; $p < 0.05$), with oxygen consumption rates lower at all values of $\Delta\Psi_m$.

463

464 **Discussion**

465 In this rodent model of sepsis and multi-organ failure, we have shown early muscle
466 dysfunction and fatigue associated with metabolic suppression, lower mitochondrial
467 membrane potential and phosphorylation capacity, but no change in mitochondrial proton
468 leak despite an increase in UCP3 protein abundance. These changes were unaffected by
469 presence or absence of UCP3 protein.

470 The pathophysiology of multi-organ failure and muscle dysfunction in established
471 sepsis is complex and multifactorial. Recent interest has focused on bioenergetic
472 dysfunction: increased production of reactive oxygen species results in disruption of
473 metabolic processes and cell damage (12, 13, 61), while decreased transcription of
474 mitochondrial proteins affects respiratory capacity (18, 32). A decrease in cell metabolism
475 may also occur for other reasons, e.g. secondary to a decrease in thyroid activity associated
476 with critical illness (9).

477 Recent publications have highlighted limitations of mouse models of sepsis and the
478 lack of translation of successful treatments from animal models to humans (31, 56). Indeed,

479 significant disparity was reported between mice and humans in their gene expression profile
480 response to inflammatory conditions including sepsis (56). We reported marked differences
481 in the metabolic response to sepsis between rats and mice (67). As seen in the present study,
482 mice showed an early and severity-dependent hypometabolic, hypothermic phenotype with
483 early myocardial depression. This presentation is seen in approximately 10% of cases of
484 human sepsis, and is associated with a 2-3 fold increased risk of mortality (4, 19). However,
485 the ability to define the roles of specific genes by genetic manipulation and to study fully
486 intact biological systems in complex diseases justify an ongoing role for rodent models in
487 defining pathophysiological mechanisms (46). We did make considerable efforts to refine
488 and optimize our murine septic model. These included using older mice equivalent to 30-40
489 year old humans (63), injecting a standardized septic inoculum, providing regular fluid
490 administration to limit hypovolemia-induced tissue hypoperfusion, and performing a block
491 randomization for group allocation in experiments (67).

492 Metabolic suppression and hypothermia are well-described phenomena in septic mice,
493 and are influenced by age, septic insult and ambient temperature (22, 54, 62, 67). We
494 previously demonstrated that rewarming of septic mice to normothermia failed to increase
495 metabolic rate (67), implying a primary metabolic suppression rather than a reactive
496 response to hypothermia.

497 UCP3 is upregulated in sepsis (60, 66), prompting speculation about the role of this
498 protein in decreasing mitochondrial coupling efficiency. This may however act as a negative
499 feedback loop to reduce ROS production (11). We set out to establish the importance and
500 functional consequence of this increase in UCP3 expression, but instead report no detectable
501 differences in the responses of *Ucp3*^(-/-) mice to sepsis. Rather than detecting effects on
502 mitochondrial proton leak, our findings suggest that processes related to mitochondrial
503 phosphorylation may be affected.

504 Previous studies in healthy *Ucp3*^(-/-) mice also found little difference in
505 thermoregulation and oxygen consumption rate compared to their wild-type controls (6, 64).
506 Despite a 5-fold increase in skeletal muscle UCP3 in mice given intraperitoneal endotoxin, Yu
507 *et al* in fact described a drop in core temperature to 30°C (66). While we too observed an
508 increase in skeletal muscle UCP3, we found no impact of the lack of UCP-3 protein upon
509 metabolic changes, temperature, cardiovascular and muscle function, or mortality in sepsis.
510 Similarly, while skeletal muscle mitochondria isolated from healthy *Ucp3*^(-/-) mice showed
511 more coupled respiration and increased ROS production (64), we could find no differences in
512 force, power and response to repeated stimulation between diaphragm muscle strips
513 isolated from septic wild-type and *Ucp3*^(-/-) mice. The original description of the *Ucp3*^(-/-)
514 mouse showed no compensatory up-regulation of other UCPs (64), although it is conceivable
515 that such up-regulation may be seen with sepsis. In line with previous work, we were unable
516 to detect UCP2 in muscle from either sham or septic mice using a number of commercially
517 available UCP2 antibodies (data not shown).

518 We imposed repeated work-loop cycles to mimic *in vivo* diaphragm muscle activity to
519 assess muscle fatigue (59). To our knowledge, the present study is the first description of this
520 functional assessment in a septic model. The plots show a characteristic three-phase
521 response (39); the second phase, a quasi-plateau phase of reduced function, involves
522 recruitment of oxidative metabolism and ends with depletion of high-energy substrates and
523 accumulation of phosphate and other end-products of metabolism (5). We found that this
524 second phase was significantly shorter in septic mice, was affected by hypoxia (data not
525 shown) but was independent of UCP-3 protein expression. This finding supports the notion
526 of linkage between disorders of oxidative metabolism and an inability to maintain high levels
527 of energy substrate.

528 A significantly lower $\Delta\psi_m$ was seen in the diaphragmatic myocytes of septic mice.
529 While previously shown in cells (1, 55), to our knowledge this is the first demonstration of

530 altered mitochondrial membrane potential in sepsis in a complex muscle preparation. The
531 low $\Delta\psi_m$ was a consistent finding in the septic mice, and suggests either a decreased rate of
532 $\Delta\psi_m$ generation (e.g. due to a respiratory chain defect) or an increase in turnover of
533 pathways that dissipate the gradient such as proton leak or ATP production (23). Blocking
534 ATP synthase with oligomycin increased fluorescence and hence $\Delta\psi_m$. This rise was
535 significant in the septic group and suggests higher ATP turnover in these diaphragm muscle
536 cells. This was an unexpected finding as previous studies had shown lower respiratory
537 complex activity and lower oxygen consumption in tissues and cells taken from septic
538 animals and humans (13, 16, 20).

539 Our interrogation of kinetic pathways involved in the maintenance of $\Delta\psi_m$ implies
540 that the mitochondrial pathway that generates $\Delta\psi_m$ through succinate oxidation was
541 unaffected in this model of sepsis. Substrate oxidation rates of mitochondria isolated from
542 starved sham mice were depressed at all values of $\Delta\psi_m$ compared to the other groups. This
543 implies either an altered sensitivity of these mitochondria to FCCP and/or that metabolic
544 adaptations in sepsis do not simply reflect a stressed nutritional state. Previous descriptions
545 of mitochondrial function in sepsis suggest Complex I dysfunction (12, 13). While a full kinetic
546 description of NADH-linked substrate oxidation kinetics was not attempted here due to
547 technical constraints, neither state 3 nor state 4 respiration were significantly different
548 between groups when the mitochondria were energized with complex 1 substrates pyruvate
549 and malate.

550 Proton leak kinetics were unaffected by the septic insult, despite the rise in UCP3
551 protein levels in the septic mice, although these experiments were not repeated in the
552 presence of free fatty acids or GDP (47). However, ATP turnover kinetics were significantly
553 affected in the septic mice with lower oxygen consumption rates at given values of $\Delta\psi_m$
554 when mitochondria were phosphorylating ADP. Defects in ATP synthase in sepsis have been

555 described previously and may explain these observations (16, 37, 43, 52). The higher ATP
556 turnover in the diaphragms of septic mice suggested by the $\Delta\Psi_m$ experiments, in conjunction
557 with the altered ATP turnover kinetics seen in muscle mitochondria isolated from septic mice
558 may explain, at least in part, the earlier fatigue observed in the diaphragm muscle strip
559 studies.

560 An issue to consider with the use of isolated mitochondria, especially in conditions
561 such as sepsis, is that removal from their usual cellular environment takes away the impact
562 of local regulatory processes and high levels of inflammatory mediators, and also exposes
563 them to a supranormal oxygen milieu. Such regulatory processes include energy-consuming
564 pathways, resulting in altered ATP demand, or pathways that impose control over substrate
565 trafficking into the mitochondria and substrate oxidation, thereby regulating respiratory
566 chain function and, ultimately, ATP synthesis (14). Nitric oxide, pyruvate dehydrogenase
567 kinase-4 (PDK4) and hypoxia inducible factor-1 α (HIF-1 α) are all implicated in sepsis (3, 12,
568 49); these likely continue to impose control over mitochondrial function in the intact cell and
569 tissues. Following mitochondrial isolation and washing, and exposure to hyperoxic
570 conditions, such control may be lost. A comparison of our findings using *in situ* and isolated
571 mitochondria implies that sepsis modifies both local regulatory processes and the oxidative
572 phosphorylation machinery itself. These functional changes were not associated with
573 swollen or ruptured mitochondria in an examination of electron micrographs of diaphragm
574 muscles from a limited number of sham and septic mice (data not shown). Although, no
575 formal morphological examination of these were carried out, no gross changes in the shape,
576 size or distribution of mitochondria were noted.

577 In summary, the long-term, resuscitated septic mouse model that we have described
578 exhibits metabolic suppression, hypothermia and decreased cardiovascular activity.
579 Diaphragm muscle strips from septic mice exhibit increased fatiguability *ex vivo*; this may be

580 related in part to mitochondrial dysfunction. Despite increased UCP3 protein abundance in
581 sepsis, kinetic analysis of isolated mitochondria from skeletal muscle revealed that proton
582 leak kinetics were not different from sham controls, while the lack of UCP3 protein did not
583 impact on mortality, physiological changes or muscle functionality. However, ATP turnover
584 kinetics were significantly altered, implying a defect with ATP synthesis at the level of the
585 F_0F_1 synthase or an associated transport process.

586

587 **Acknowledgements**

588 We are grateful for the technical help and assistance of Raymond Stidwill and
589 Valerie Taylor with the septic model.

590 **Grants**

591 This work was funded by a MRC Clinical Research Fellowship grant for PSZ.

592 **Disclosures**

593 There are no conflicts of interest to report.

594

595

596 **References**

- 597 1. **Adrie C, Bachelet M, Vayssier-Taussat M, Russo-Marie F, Bouchaert I,**
598 **Adib-Conquy M, Cavaillon JM, Pinsky MR, Dhainaut JF, and Polla BS.**
599 Mitochondrial membrane potential and apoptosis peripheral blood monocytes in
600 severe human sepsis. *American journal of respiratory and critical care medicine*
601 164: 389-395, 2001.
- 602 2. **Affourtit C, Quinlan CL, and Brand MD.** Measurement of proton leak and
603 electron leak in isolated mitochondria. *Methods in molecular biology (Clifton, NJ)*
604 810: 165-182, 2012.
- 605 3. **Alamdari N, Constantin-Teodosiu D, Murton AJ, Gardiner SM, Bennett**
606 **T, Layfield R, and Greenhaff PL.** Temporal changes in the involvement of
607 pyruvate dehydrogenase complex in muscle lactate accumulation during
608 lipopolysaccharide infusion in rats. *The Journal of physiology* 586: 1767-1775,
609 2008.
- 610 4. **Arons MM, Wheeler AP, Bernard GR, Christman BW, Russell JA,**
611 **Schein R, Summer WR, Steinberg KP, Fulkerson W, Wright P, Dupont WD,**
612 **and Swindell BB.** Effects of ibuprofen on the physiology and survival of
613 hypothermic sepsis. Ibuprofen in Sepsis Study Group. *Critical Care Medicine* 27:
614 699-707, 1999.
- 615 5. **Barclay CJ, Constable JK, and Gibbs CL.** Energetics of fast- and slow-
616 twitch muscles of the mouse. *The Journal of physiology* 472: 61-80, 1993.
- 617 6. **Barclay CJ, Woledge RC, and Curtin NA.** Effects of UCP3 genotype,
618 temperature and muscle type on energy turnover of resting mouse skeletal
619 muscle. *Pflügers Archiv : European journal of physiology* 457: 857-864, 2009.
- 620 7. **Batt J, dos Santos CC, Cameron JI, and Herridge MS.** Intensive care unit-
621 acquired weakness: clinical phenotypes and molecular mechanisms. *American*
622 *journal of respiratory and critical care medicine* 187: 238-246, 2013.
- 623 8. **Bhattacharya SK, Thakar JH, Johnson PL, and Shanklin DR.** Isolation of
624 skeletal muscle mitochondria from hamsters using an ionic medium containing
625 ethylenediaminetetraacetic acid and nagarse. *Analytical Biochemistry* 192: 344-
626 349, 1991.
- 627 9. **Boelen A, Kwakkel J, and Fliers E.** Beyond low plasma T3: local thyroid
628 hormone metabolism during inflammation and infection. *Endocrine reviews* 32:
629 670-693, 2011.
- 630 10. **Brand MD.** The proton leak across the mitochondrial inner membrane.
631 *Biochimica et biophysica acta* 1018: 128-133, 1990.
- 632 11. **Brand MD and Esteves TC.** Physiological functions of the mitochondrial
633 uncoupling proteins UCP2 and UCP3. *Cell Metabolism* 2: 85-93, 2005.
- 634 12. **Brealey D, Brand M, Hargreaves I, Heales S, Land J, Smolenski R,**
635 **Davies NA, Cooper CE, and Singer M.** Association between mitochondrial
636 dysfunction and severity and outcome of septic shock. *Lancet* 360: 219-223,
637 2002.
- 638 13. **Brealey D, Karyampudi S, Jacques TS, Novelli M, Stidwill R, Taylor V,**
639 **Smolenski RT, and Singer M.** Mitochondrial dysfunction in a long-term rodent
640 model of sepsis and organ failure. *American journal of physiology Regulatory,*
641 *integrative and comparative physiology* 286: R491-497, 2004.

- 642 14. **Brown GC.** Control of respiration and ATP synthesis in mammalian
643 mitochondria and cells. *The Biochemical journal* 284 (Pt 1): 1-13, 1992.
- 644 15. **Brown GC and Cooper CE.** *Bioenergetics: A practical approach*: IRL Press,
645 1995.
- 646 16. **Callahan LA and Supinski GS.** Sepsis induces diaphragm electron
647 transport chain dysfunction and protein depletion. *American journal of*
648 *respiratory and critical care medicine* 172: 861-868, 2005.
- 649 17. **Campanella M, Parker N, Tan CH, Hall AM, and Duchen MR.** IF(1):
650 setting the pace of the F(1)F(o)-ATP synthase. *Trends in biochemical sciences* 34:
651 343-350, 2009.
- 652 18. **Carré JE, Orban J-C, Re L, Felsmann K, Iffert W, Bauer M, Suliman HB,**
653 **Piantadosi CA, Mayhew TM, Breen P, Stotz M, and Singer M.** Survival in
654 critical illness is associated with early activation of mitochondrial biogenesis.
655 *American journal of respiratory and critical care medicine* 182: 745-751, 2010.
- 656 19. **Clemmer TP, Fisher CJ, Bone RC, Slotman GJ, Metz CA, and Thomas**
657 **FO.** Hypothermia in the sepsis syndrome and clinical outcome. The
658 Methylprednisolone Severe Sepsis Study Group. *Critical Care Medicine* 20: 1395-
659 1401, 1992.
- 660 20. **Crouser ED, Julian MW, Blaho DV, and Pfeiffer DR.** Endotoxin-induced
661 mitochondrial damage correlates with impaired respiratory activity. *Critical Care*
662 *Medicine* 30: 276-284, 2002.
- 663 21. **De Jonghe B, Sharshar T, Lefaucheur J-P, Authier F-J, Durand-Zaleski**
664 **I, Boussarsar M, Cerf C, Renaud E, Mesrati F, Carlet J, Raphaël J-C, Outin H,**
665 **Bastuji-Garin S, and Réanimation GdRedaEdNe.** Paresis acquired in the
666 intensive care unit: a prospective multicenter study. *JAMA : the journal of the*
667 *American Medical Association* 288: 2859-2867, 2002.
- 668 22. **Dogan MD, Ataoglu H, and Akarsu ES.** Effects of different serotypes of
669 *Escherichia coli* lipopolysaccharides on body temperature in rats. *Life sciences*
670 67: 2319-2329, 2000.
- 671 23. **Duchen MR.** Mitochondria in health and disease: perspectives on a new
672 mitochondrial biology. *Molecular aspects of medicine* 25: 365-451, 2004.
- 673 24. **Duchen MR, Surin A, and Jacobson J.** Imaging mitochondrial function in
674 intact cells. *Methods in enzymology* 361: 353-389, 2003.
- 675 25. **Echtay KS, Roussel D, St-Pierre J, Jekabsons MB, Cadenas S, Stuart JA,**
676 **Harper JA, Roebuck SJ, Morrison A, Pickering S, Clapham JC, and Brand MD.**
677 Superoxide activates mitochondrial uncoupling proteins. *Nature* 415: 96-99,
678 2002.
- 679 26. **Fredriksson K, Hammarqvist F, Strigård K, Hultenby K, Ljungqvist O,**
680 **Wernerman J, and Rooyackers O.** Derangements in mitochondrial metabolism
681 in intercostal and leg muscle of critically ill patients with sepsis-induced multiple
682 organ failure. *American journal of physiology Endocrinology and metabolism* 291:
683 E1044-1050, 2006.
- 684 27. **Frost MT, Wang Q, Moncada S, and Singer M.** Hypoxia accelerates nitric
685 oxide-dependent inhibition of mitochondrial complex I in activated macrophages.
686 *American journal of physiology Regulatory, integrative and comparative physiology*
687 288: R394-400, 2005.
- 688 28. **Garedew A, Henderson SO, and Moncada S.** Activated macrophages
689 utilize glycolytic ATP to maintain mitochondrial membrane potential and prevent
690 apoptotic cell death. *Cell Death and Differentiation* 17: 1540-1550, 2010.

- 691 29. **Gong DW, Monemdjou S, GavriloVA O, Leon LR, Marcus-Samuels B,**
692 **Chou CJ, Everett C, Kozak LP, Li C, Deng C, Harper ME, and Reitman ML.** Lack
693 of obesity and normal response to fasting and thyroid hormone in mice lacking
694 uncoupling protein-3. *The Journal of biological chemistry* 275: 16251-16257,
695 2000.
- 696 30. **Griffiths RD and Hall JB.** Intensive care unit-acquired weakness. *Critical*
697 *Care Medicine* 38: 779-787, 2010.
- 698 31. **Hackam DG and Redelmeier DA.** Translation of research evidence from
699 animals to humans. *JAMA : the journal of the American Medical Association* 296:
700 1731-1732, 2006.
- 701 32. **Haden DW, Suliman HB, Carraway MS, Welty-Wolf KE, Ali AS, Shitara**
702 **H, Yonekawa H, and Piantadosi CA.** Mitochondrial biogenesis restores
703 oxidative metabolism during Staphylococcus aureus sepsis. *American journal of*
704 *respiratory and critical care medicine* 176: 768-777, 2007.
- 705 33. **Hermans G, De Jonghe B, Bruyninckx F, and Van den Berghe G.** Clinical
706 review: Critical illness polyneuropathy and myopathy. *Critical care (London,*
707 *England)* 12: 238, 2008.
- 708 34. **Iwashyna TJ, Ely EW, Smith DM, and Langa KM.** Long-term cognitive
709 impairment and functional disability among survivors of severe sepsis. *JAMA : the*
710 *journal of the American Medical Association* 304: 1787-1794, 2010.
- 711 35. **Jastroch M, Divakaruni AS, Mookerjee S, Treberg JR, and Brand MD.**
712 Mitochondrial proton and electron leaks. *Essays in Biochemistry* 47: 53-67, 2010.
- 713 36. **Jéquier E, Acheson K, and Schutz Y.** Assessment of energy expenditure
714 and fuel utilization in man. *Annual review of nutrition* 7: 187-208, 1987.
- 715 37. **Kantrow SP, Taylor DE, Carraway MS, and Piantadosi CA.** Oxidative
716 metabolism in rat hepatocytes and mitochondria during sepsis. *Archives of*
717 *biochemistry and biophysics* 345: 278-288, 1997.
- 718 38. **Kress JP and Hall JB.** ICU-acquired weakness and recovery from critical
719 illness. *The New England journal of medicine* 370: 1626-1635, 2014.
- 720 39. **Lännergren J and Westerblad H.** Force decline due to fatigue and
721 intracellular acidification in isolated fibres from mouse skeletal muscle. *The*
722 *Journal of physiology* 434: 307-322, 1991.
- 723 40. **Latronico N and Bolton CF.** Critical illness polyneuropathy and
724 myopathy: a major cause of muscle weakness and paralysis. *The Lancet*
725 *Neurology* 10: 931-941, 2011.
- 726 41. **Lionetti L, Iossa S, Brand MD, and Liverini G.** Relationship between
727 membrane potential and respiration rate in isolated liver mitochondria from rats
728 fed an energy dense diet. *Molecular and cellular biochemistry* 158: 133-138, 1996.
- 729 42. **Mailloux RJ and Harper M-E.** Mitochondrial proticity and ROS signaling:
730 lessons from the uncoupling proteins. *Trends in endocrinology and metabolism:*
731 *TEM* 23: 451-458, 2012.
- 732 43. **Mela L, Bacalzo LV, and Miller LD.** Defective oxidative metabolism of rat
733 liver mitochondria in hemorrhagic and endotoxin shock. *The American journal of*
734 *physiology* 220: 571-577, 1971.
- 735 44. **Nicholls DG.** A history of UCP1. *Biochemical Society transactions* 29: 751-
736 755, 2001.
- 737 45. **Nicholls DG and Ferguson SJ.** *Bioenergetics (Third Edition)*, 2002.
- 738 46. **Osuchowski MF, Remick DG, Lederer JA, Lang CH, Aasen AO, Aibiki M,**
739 **Azevedo LC, Bahrami S, Boros M, Cooney R, Cuzzocrea S, Jiang Y, Junger WG,**

740 **Hirasawa H, Hotchkiss RS, Li X-A, Radermacher P, Redl H, Salomao R,**
741 **Soebandrio A, Thiemermann C, Vincent J-L, Ward P, Yao Y-M, Yu H-P,**
742 **Zingarelli B, and Chaudry IH.** Abandon the mouse research ship? Not just yet!
743 *Shock (Augusta, Ga)* 41: 463-475, 2014.

744 47. **Parker N, Affourtit C, Vidal-Puig A, and Brand MD.** Energization-
745 dependent endogenous activation of proton conductance in skeletal muscle
746 mitochondria. *The Biochemical journal* 412: 131-139, 2008.

747 48. **Parker N, Vidal-Puig A, and Brand MD.** Stimulation of mitochondrial
748 proton conductance by hydroxynonenal requires a high membrane potential.
749 *Bioscience reports* 28: 83-88, 2008.

750 49. **Peyssonnaud C, Cejudo-Martin P, Doedens A, Zinkernagel AS, Johnson**
751 **RS, and Nizet V.** Cutting edge: Essential role of hypoxia inducible factor-1alpha
752 in development of lipopolysaccharide-induced sepsis. *Journal of immunology*
753 *(Baltimore, Md : 1950)* 178: 7516-7519, 2007.

754 50. **Puthuchery Z, Harridge S, and Hart N.** Skeletal muscle dysfunction in
755 critical care: wasting, weakness, and rehabilitation strategies. *Critical Care*
756 *Medicine* 38: S676-682, 2010.

757 51. **Rasmussen HN and Rasmussen UF.** Small scale preparation of skeletal
758 muscle mitochondria, criteria of integrity, and assays with reference to tissue
759 function. *Molecular and cellular biochemistry* 174: 55-60, 1997.

760 52. **Robichaud S, Lalu M, Udenberg T, Schulz R, and Sawicki G.** Proteomics
761 analysis of changes in myocardial proteins during endotoxemia. *Journal of*
762 *Proteomics* 72: 648-655, 2009.

763 53. **Rolfe DF and Brown GC.** Cellular energy utilization and molecular origin
764 of standard metabolic rate in mammals. *Physiological reviews* 77: 731-758, 1997.

765 54. **Rudaya AY, Steiner AA, Robbins JR, Dragic AS, and Romanovsky AA.**
766 Thermoregulatory responses to lipopolysaccharide in the mouse: dependence on
767 the dose and ambient temperature. *American journal of physiology Regulatory,*
768 *integrative and comparative physiology* 289: R1244-1252, 2005.

769 55. **Růzicka M, Skobisová E, Dlasková A, Santorová J, Smolková K, Spacek**
770 **T, Zácková M, Modrianský M, and Jezek P.** Recruitment of mitochondrial
771 uncoupling protein UCP2 after lipopolysaccharide induction. *The international*
772 *journal of biochemistry & cell biology* 37: 809-821, 2005.

773 56. **Seok J, Warren HS, Cuenca AG, Mindrinos MN, Baker HV, Xu W,**
774 **Richards DR, McDonald-Smith GP, Gao H, Hennessy L, Finnerty CC, López**
775 **CM, Honari S, Moore EE, Minei JP, Cuschieri J, Bankey PE, Johnson JL, Sperry**
776 **J, Nathens AB, Billiar TR, West MA, Jeschke MG, Klein MB, Gamelli RL,**
777 **Gibran NS, Brownstein BH, Miller-Graziano C, Calvano SE, Mason PH, Cobb**
778 **JP, Rahme LG, Lowry SF, Maier RV, Moldawer LL, Herndon DN, Davis RW,**
779 **Xiao W, Tompkins RG, and the Inflammation and Host Response to Injury**
780 **LSCRP.** Genomic responses in mouse models poorly mimic human inflammatory
781 diseases. *Proceedings of the National Academy of Sciences of the United States of*
782 *America*, 2013.

783 57. **Srere PA.** The citrate enzymes: their structures, mechanisms, and
784 biological functions. *Current topics in cellular regulation* 5: 229-283, 1972.

785 58. **St-Pierre J, Buckingham JA, Roebuck SJ, and Brand MD.** Topology of
786 superoxide production from different sites in the mitochondrial electron
787 transport chain. *The Journal of biological chemistry* 277: 44784-44790, 2002.

- 788 59. **Stevens ED and Faulkner JA.** The capacity of mdx mouse diaphragm
789 muscle to do oscillatory work. *The Journal of physiology* 522 Pt 3: 457-466, 2000.
- 790 60. **Sun X, Wray C, Tian X, Hasselgren P-O, and Lu J.** Expression of
791 uncoupling protein 3 is upregulated in skeletal muscle during sepsis. *American*
792 *journal of physiology Endocrinology and metabolism* 285: E512-520, 2003.
- 793 61. **Supinski GS and Callahan LA.** Free radical-mediated skeletal muscle
794 dysfunction in inflammatory conditions. *Journal of applied physiology (Bethesda,*
795 *Md : 1985)* 102: 2056-2063, 2007.
- 796 62. **Tateda K, Matsumoto T, Miyazaki S, and Yamaguchi K.**
797 Lipopolysaccharide-induced lethality and cytokine production in aged mice.
798 *Infection and immunity* 64: 769-774, 1996.
- 799 63. **Turnbull IR, Wlzonek JJ, Osborne D, Hotchkiss RS, Coopersmith CM,**
800 **and Buchman TG.** Effects of age on mortality and antibiotic efficacy in cecal
801 ligation and puncture. *Shock (Augusta, Ga)* 19: 310-313, 2003.
- 802 64. **Vidal-Puig AJ, Grujic D, Zhang CY, Hagen T, Boss O, Ido Y, Szczepanik**
803 **A, Wade J, Mootha V, Cortright R, Muoio DM, and Lowell BB.** Energy
804 metabolism in uncoupling protein 3 gene knockout mice. *The Journal of biological*
805 *chemistry* 275: 16258-16266, 2000.
- 806 65. **Woledge RC and Curtin NA.** The efficiency of energy conversion by
807 swimming muscles of fish. *Advances in experimental medicine and biology* 332:
808 735-743; discussion 744-737, 1993.
- 809 66. **Yu XX, Barger JL, Boyer BB, Brand MD, Pan G, and Adams SH.** Impact of
810 endotoxin on UCP homolog mRNA abundance, thermoregulation, and
811 mitochondrial proton leak kinetics. *American journal of physiology Endocrinology*
812 *and metabolism* 279: E433-446, 2000.
- 813 67. **Zolfaghari PS, Pinto BB, Dyson A, and Singer M.** The metabolic
814 phenotype of rodent sepsis: cause for concern. *Intensive Care Med Exp in press*
815 *OpenURL*, 2013.
- 816
- 817
- 818

819 **Figure legends**

820 **Figure 1** Simplified illustration of mitochondrial bioenergetic pathways split into three groups
821 of reactions: 1) reactions that generate $\Delta\psi_m$ (substrate kinetics), 2) reactions consuming $\Delta\psi_m$
822 to generate ATP (phosphorylation kinetics), and 3) reactions that consume $\Delta\psi_m$ without
823 generating ATP (leak kinetics). Adapted from Nicholls & Ferguson 2002.

824

825 **Figure 2** Survival curve of wild-type (n=11) and UCP3^(-/-) mice (n=12) after i/p injection of
826 fecal slurry. Sham mice (10 wild-type, 9 UCP3^(-/-)) received i/p saline. All animals received s/c
827 fluids at 0, 6, 18, 30 and 42 hour time-points.

828

829 **Figure 3** Temperature (A) and oxygen consumption (B) of wild-type and UCP3^(-/-) mice
830 following induction of sepsis (or sham controls). (C) Plot of oxygen consumption against core
831 temperature of wild-type and UCP3^(-/-) mice. Line of best fit and correlation coefficient are
832 noted on the graph. (D) Percentage weight change of sham and septic mice over 24 hours.
833 Statistical significance (p<0.05) was seen between groups in each genotype. All mice received
834 s/c fluid at 0, 6 and 18h time-points; food was withdrawn from starved sham mice
835 immediately after i/p injection of saline.

836 * p<0.05 compared to fed sham using two-way ANOVA for temperature data over time, and
837 one-way ANOVA for weight data.

838

839

840 **Figure 4** Echocardiography results of wild-type and Ucp3^(-/-) mice following i/p injection of
841 fecal slurry or n-saline. All septic mice were in the severe category according to the clinical
842 scoring scale. Results are mean \pm SEM. *p<0.02 comparing sham values between the two
843 genotypes; § p<0.01 comparing septic and sham values in same genotype using two-way
844 ANOVA repeated measures.

845

846 **Figure 5** (A) Maximal isometric force generated by 350ms tetanic stimulation in diaphragm
847 strips taken from wild-type and *Ucp3*^{-/-} mice and normalized to cross-sectional area. (B)
848 Power generated by the muscle strips during sinusoidal length change at 4Hz with phasic
849 tetanic stimulation simulating *in vivo* muscle function. Power is expressed relative to muscle
850 wet weight. (C) Example of a work-loop generated by muscle strips from WT fed sham,
851 starved sham and septic mice (optimal muscle lengths: 8.4mm, 9.5mm, 9.7mm; muscle dry
852 weight: 0.665mg, 0.627mg, 0.578mg, respectively). (D) Power performance of diaphragm
853 strips taken from fed sham and septic wild-type and *Ucp3*^{-/-} mice undertaking 120 repeated
854 work-loop cycles at 2Hz over a 1 minute period. Values are the average power per cycle; for
855 clarity some values are not shown. The initial rapid decline is shallower, and the first plateau
856 ends earlier (marked by broken vertical line), in the septic groups in both genotypes
857 compared to the sham group. Values are mean \pm 1 SEM.

858

859 **Figure 6** Representative Western blots of UCP-3 protein content of diaphragm muscles from
860 sham (n=6) and septic wild-type mice 24 h after injection of fecal slurry (n=8). B Mean (\pm SD)
861 densitometry values of UCP-3 protein abundance at 10 h and 24 h in diaphragm muscle.
862 Values were normalized to alpha-tubulin content. * p<0.05 compared to sham using one-way
863 ANOVA.

864

865 **Figure 7** Live-cell images of TMRM (A) and Mitotracker green (B&C) fluorescence pattern in
866 diaphragm muscle cells. Two distinct mitochondrial subpopulation of subsarcolemmal (SS)
867 and interfibrillar (IF) are seen. Characteristic double band pattern of interfibrillar
868 mitochondria is shown in B (arrowed). (C) Z-stack 3-D image projection of a diaphragm strip
869 loaded with Mitotracker Green showing muscle and pleural cells on the surface. (D) Average

870 TMRM fluorescence intensity of isolated diaphragms strips from sham and septic *wild-type*
871 mice at 24h bathed in TMRM 100nM (baseline), and after addition of oligomycin 5 $\mu\text{g/ml}$.
872 (* $p=0.016$ independent sample t-test; $\S p<0.01$ paired sample t-test comparing oligomycin to
873 baseline fluorescence in the septic group).

874

875 **Figure 8** Dependency of oxygen consumption rate on $\Delta\psi_m$ for different $\Delta\psi_m$ -producing and -
876 dissipating kinetic modules (left panels), with oxygen consumption rates at $\Delta\psi_m$ of -170mV
877 (right panels), for mitochondria isolated from total skeletal muscle of septic, fed sham and
878 fasted sham mice. A & B, proton leak kinetics; C & D, total $\Delta\psi_m$ -dissipating pathways (proton
879 leak + ATP turnover reactions) under state 3 conditions; E & F; ATP turnover kinetics
880 (phosphorylation + transport reactions) – kinetic curves derived from subtraction of A from
881 C; G & H, substrate (succinate) oxidation kinetics.

882 * $p<0.05$ one-way ANOVA significance of septic vs. both sham groups; ** $p<0.05$ one-way
883 ANOVA starved sham vs. fed sham and septic groups.

884

885

886

887 **Table 1** Blood gas and serum biochemistry at 24 hours in *wild-type* mice following
 888 induction of sepsis with comparison against sham controls.

	pH	pCO ₂ kPa	pO ₂ kPa	Lactate mmol/l	Hb g/dl	Glucose mmol/L	Urea mmol/l	Creatinine μmol/l	AST IU/l	ALT IU/l
Sham	7.33 ± 0.03	4.3 ± 0.3	13.4 ± 4.2	2.4 ± 0.9	13.2 ± 0.2	11.7 ± 4.0	6.5 ± 2.0	10 ± 6	61 ± 30	24 ± 14
Septic	6.96 ± 0.12*	8.5 ± 4.1*	12.2 ± 4.3	5.0 ± 1.2*	15.1 ± 1.6*	14.9 ± 2.4*	34 ± 28*	30±15*	266 ± 95*	77 ± 28*

889 (mean ± SD *p<0.05)

890 Hb Hemoglobin, AST Aspartate transaminase, ALT Alanine aminotransferase, IU international unit.

891

Figure 1

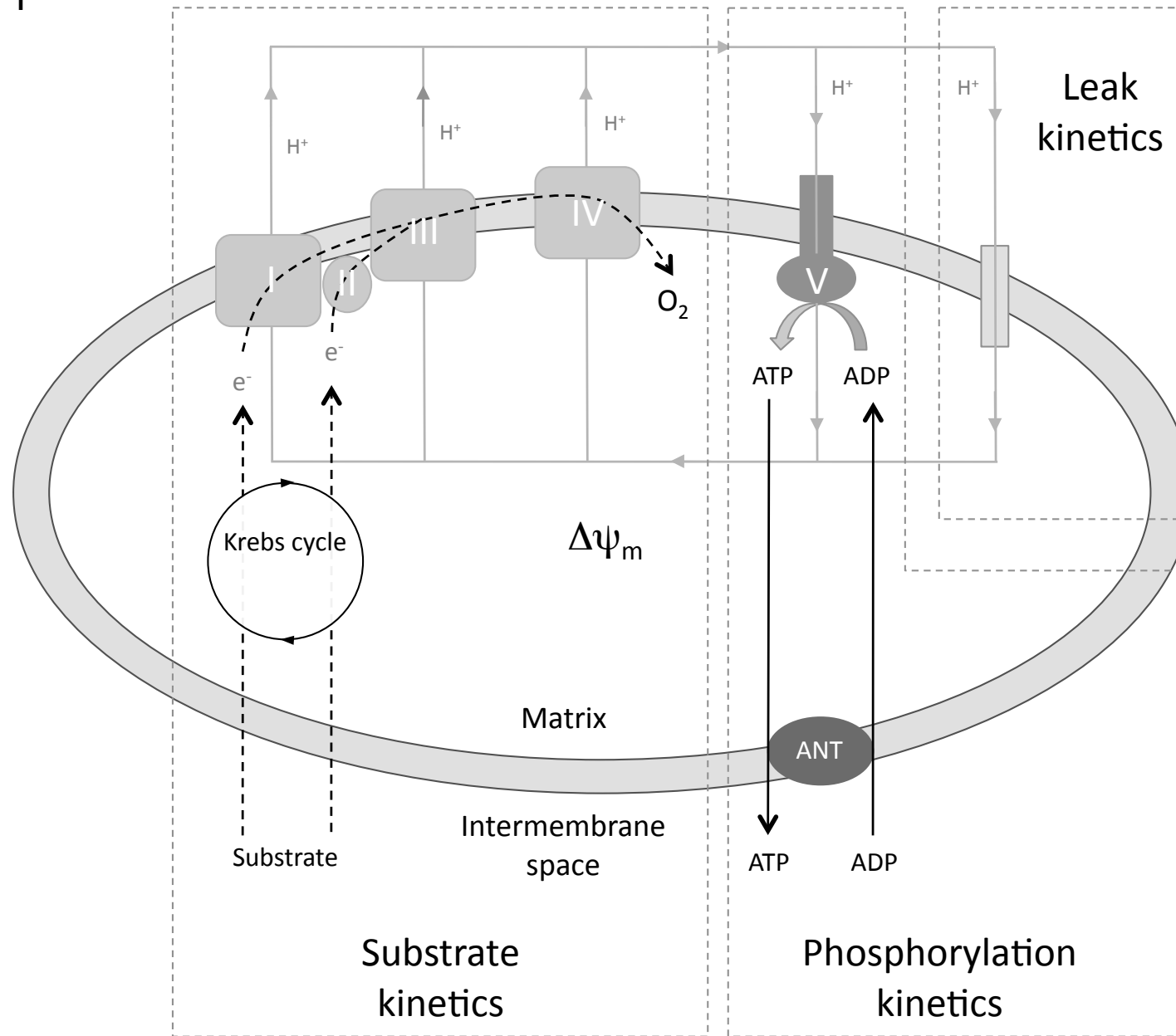


Figure 2

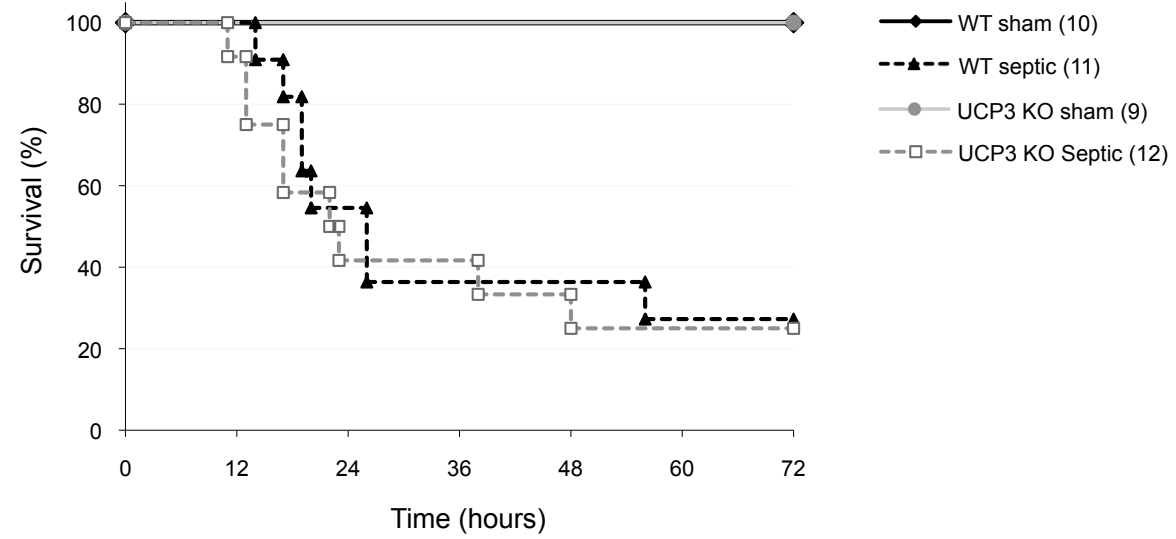


Figure 3

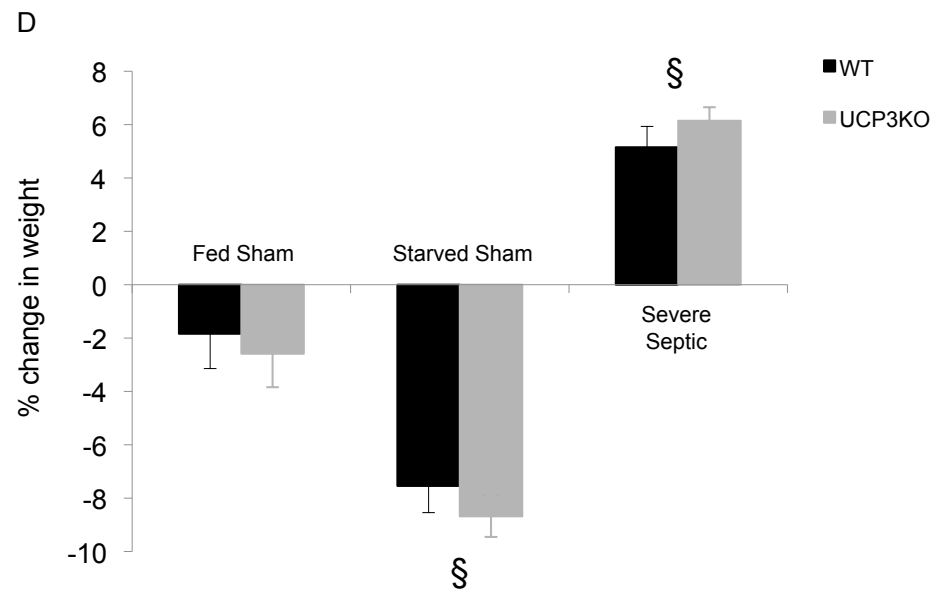
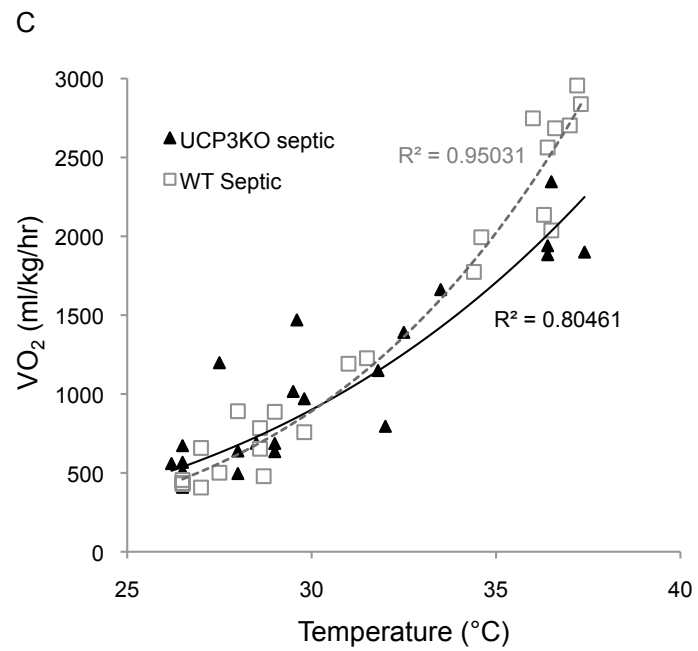
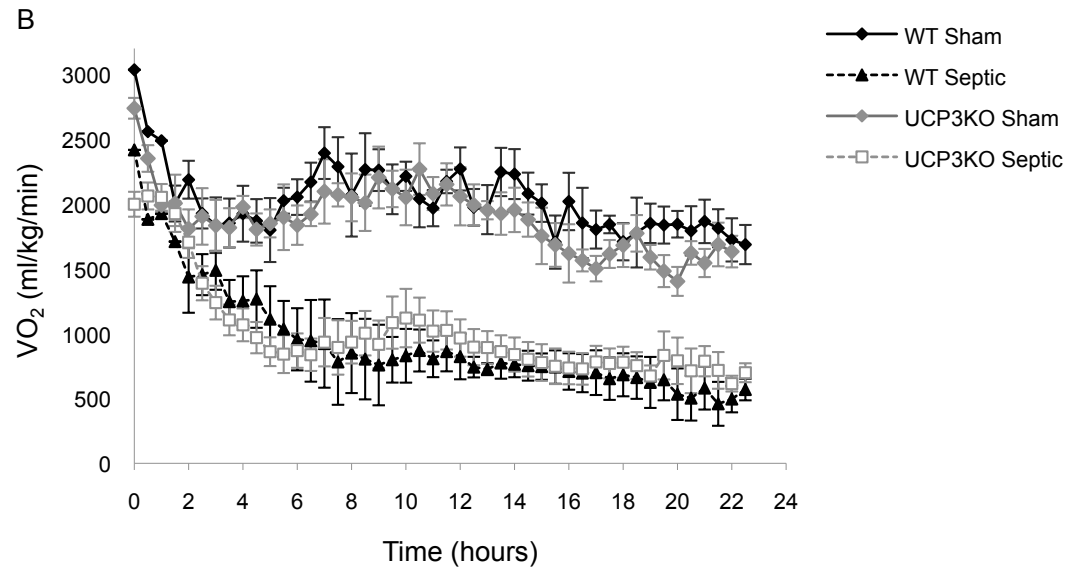
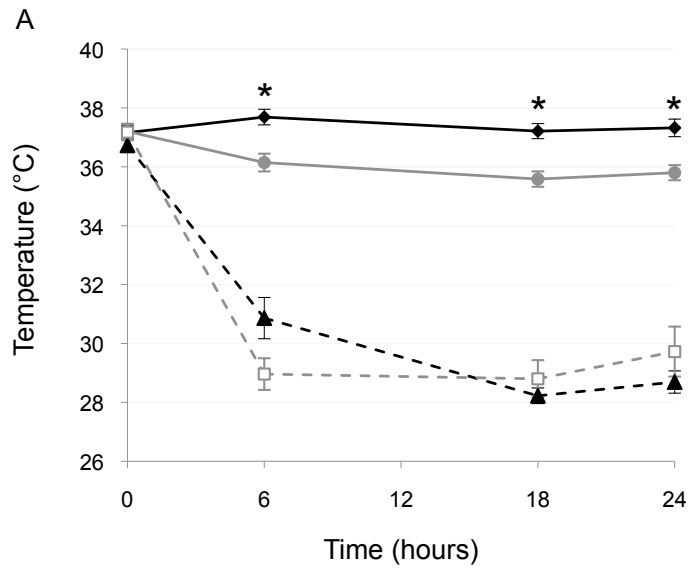


Figure 4

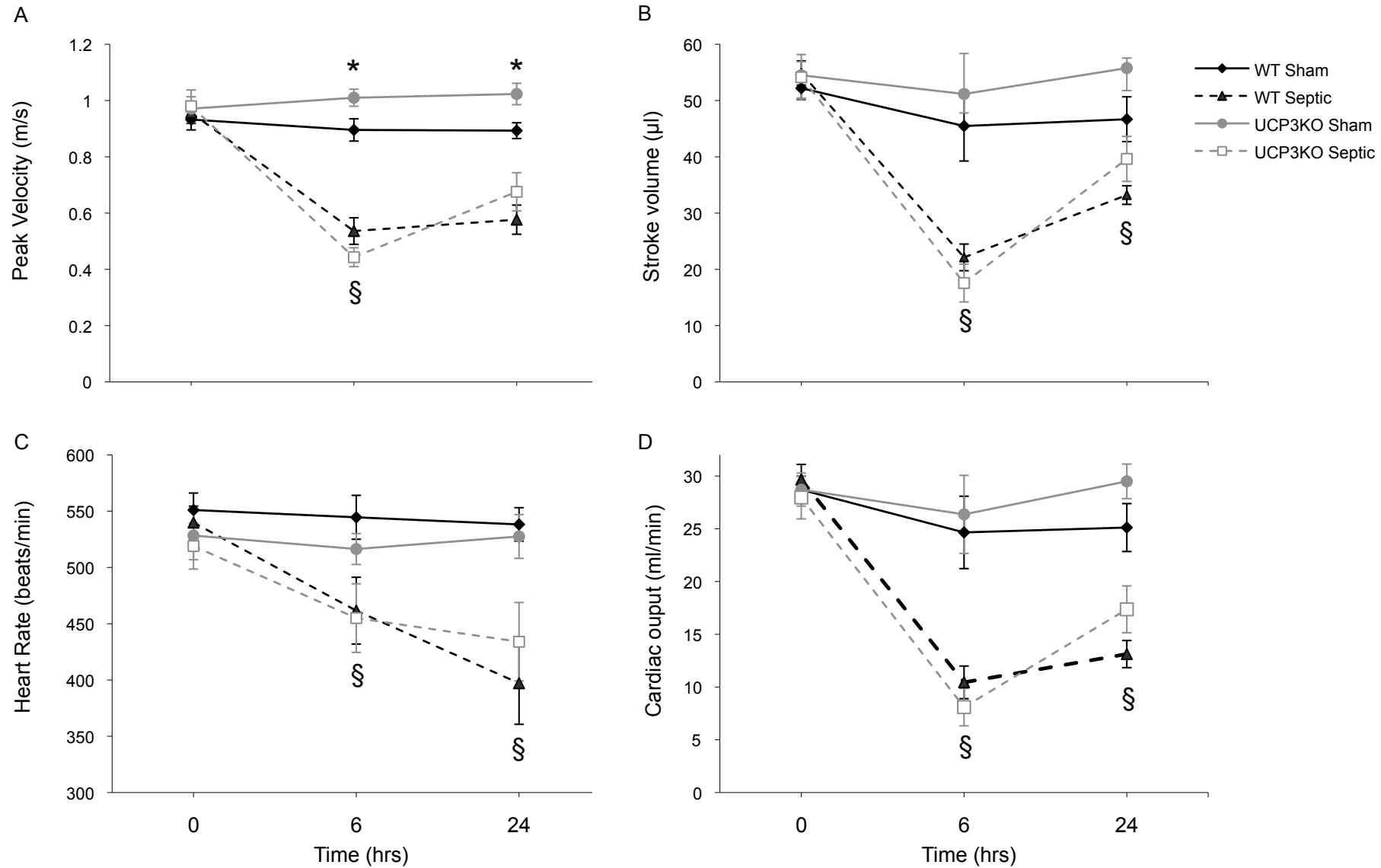


Fig 5

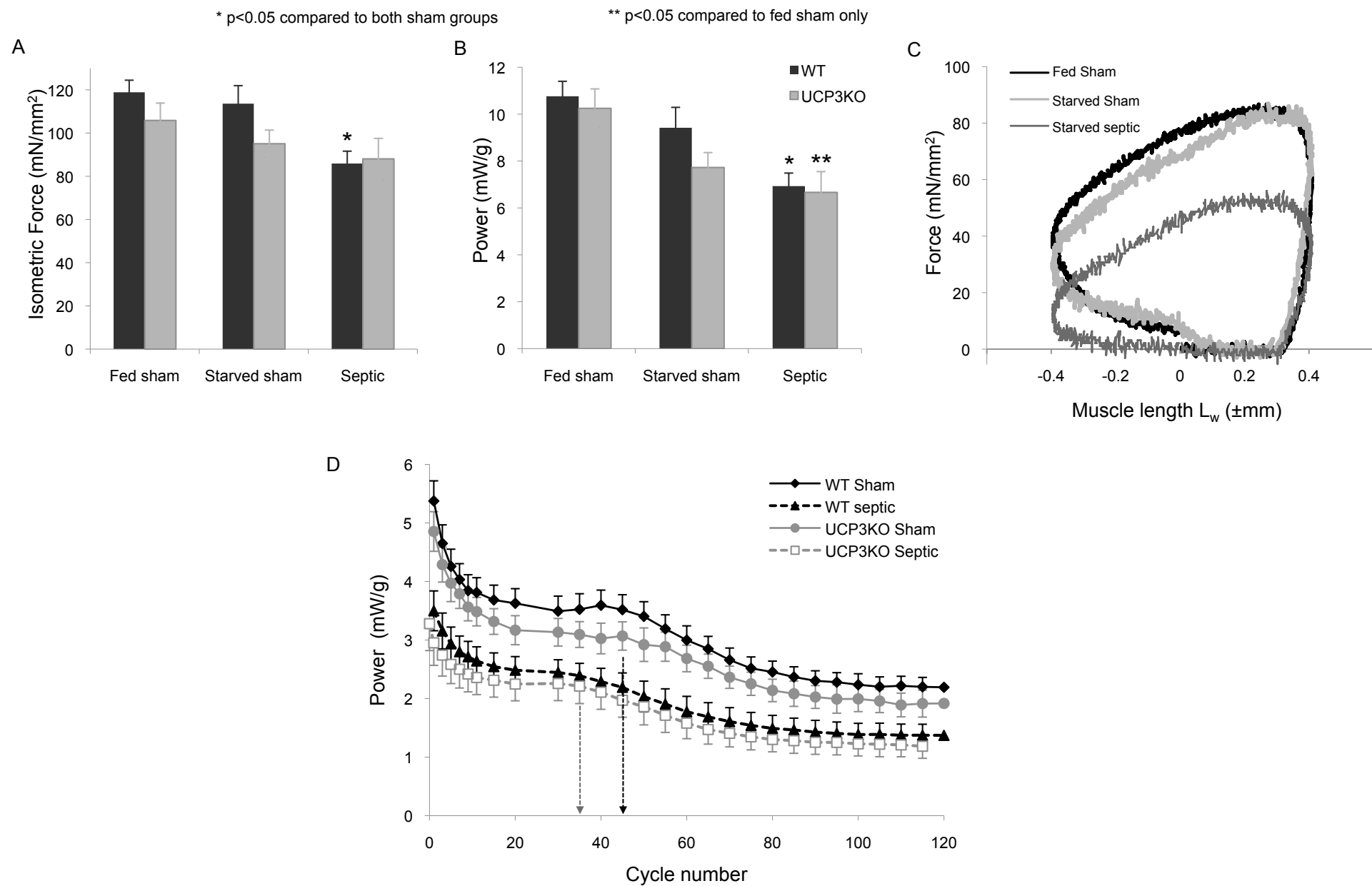


Figure 6

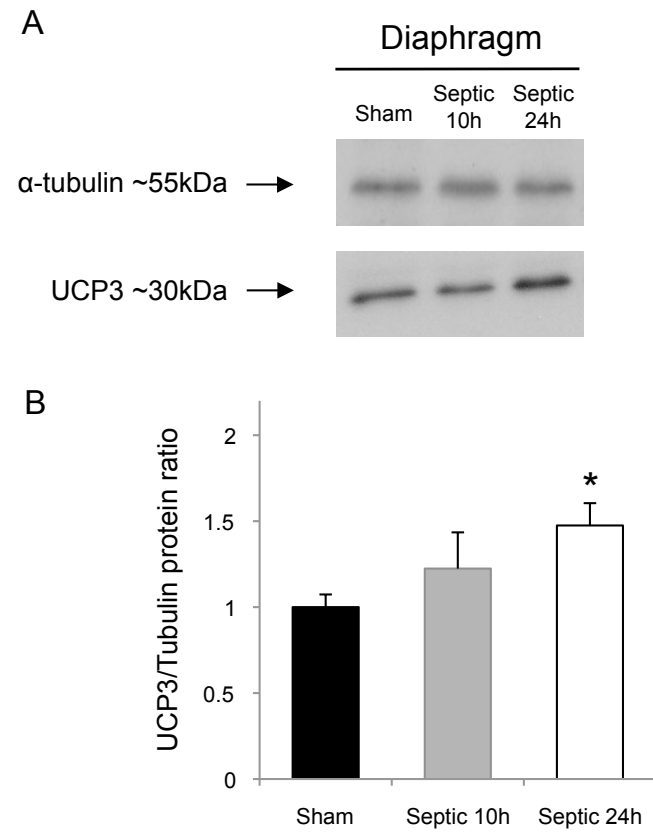


Figure 7

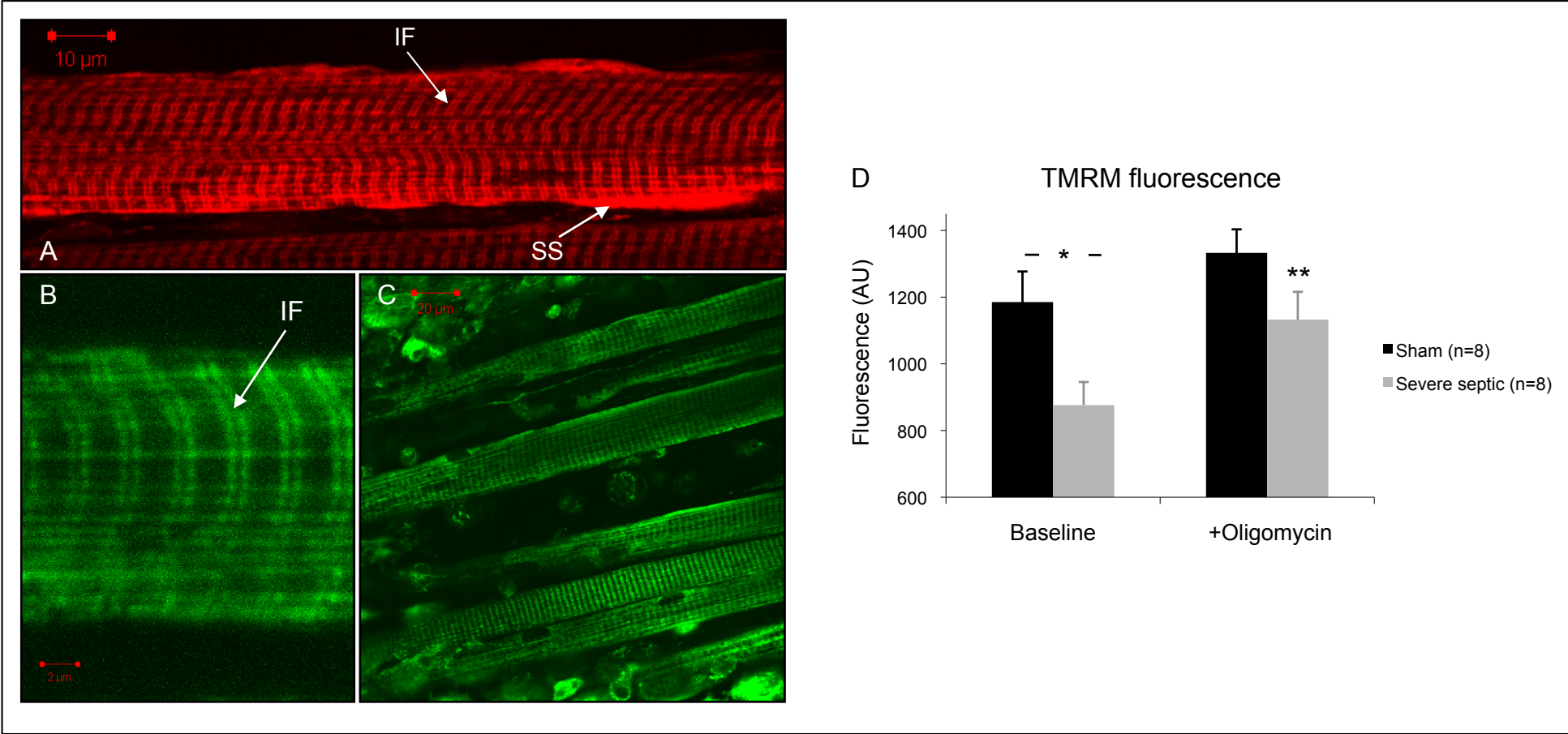


Figure 8

